Validating the Physics-Driven Lumped-Element Model of the LHC Main Dipole Magnet

M. Janitschke, M. Bednarek, E. Ravaioli, A.P. Verweij, G. Willering, M. Wozniak, and U. van Rienen, *Member, IEEE*

***Abstract*—Measuring the complex impedance of a superconducting magnet as a function of frequency provides valuable insight into its electrodynamics. In particular, the characteristic features of some non-conform behaviour, such as an insulation fault, may be easier to assess when performing impedance measurements rather than observing time-domain signals. A physics-driven equivalent circuit model of a superconducting magnet has been recently developed, whose parameters are derived using solely measured geometric and material properties. This contribution describes its validation against impedance measurements of a spare LHC superconducting main dipole, performed at the CERN magnet test facility. The proposed model includes lumped-elements capturing individual physical phenomena, such as superconducting filament magnetization, inter-filament and inter-strand coupling currents, eddy currents in the strand copper matrix and various magnet components, and stray capacitances. It is possible to predict the impact of different physical effects in different frequency ranges and compare simulations to experimental results. It is shown that the validated model can accurately reproduce the magnet's impedance in a frequency range up to 5 kHz in the different conditions considered.**

***Index Terms*—Accelerator magnet, AC-losses, frequency-domain, impedance measurements, superconducting coil.**

I. Introduction

MEASUREMENTS of the complex impedance as a function of the frequency are often used across the electrical engineering domain to better understand and describe complex systems. They can provide valuable insights into the systems' behaviour that are difficult or impossible to obtain with time-domain measurements.

Transfer Function Measurements (TFM) of superconducting magnets could be used to detect the characteristic features of some non-conform behaviour of the coil-winding pack. This was used in the past for short-circuit detection in non-planar coils in fusion stellarators [1], [2] and in CICC model coils [3] and to monitor and control the resin impregnation process in Nb_3Sn coils [4]. In order to correctly identify non-conform behaviour, it is crucial to properly understand and interpret the measured signals in a TFM. Moreover, reconstructing the magnet behaviour in an appropriate simulation model can achieve a capability to explore non-nominal behaviour and failure scenarios, which might be difficult to realize in a laboratory set-up.

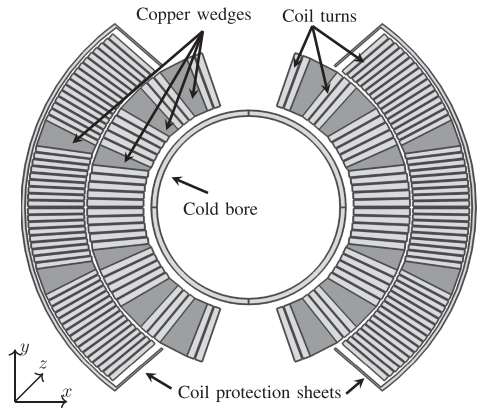

Fig. 1. Cross-section of one aperture of the LHC main dipole showing the coil turns, the copper wedges, cold-bore and coil-protection sheets.

Frequency-domain models utilizing equivalent lumped-element circuit models were previously derived [5], [6], [7], [8], [9], [10], [11]. However, these might lack physical interpretability, are not easily able to include further non-linear effects, and cannot be easily adapted to simulate non-conform behaviour such as for example inter-turn shorts in the coil winding pack.

A physics-driven equivalent circuit model of a superconducting magnet was developed, aiming to reproduce the behaviour of a superconducting magnet in the time- and frequency-domain. As such, the model includes different physical phenomena occurring in the magnet, such as superconducting filament magnetization, inter-filament and inter-strand coupling currents, eddy currents in various magnet components, and stray capacitances. The equivalent parameters used to model these phenomena are either based on analytically-derived equations or Finite-Element models (FEM).

An extensive impedance measurement campaign was recently conducted on a spare LHC main superconducting dipole at the CERN magnet test facility. This contribution describes the measurements and, utilizing the measured transfer functions, validates the derived model for the LHC superconducting main dipole in the frequency domain.

Manuscript received 25 September 2023; accepted 30 January 2024. Date of publication 19 February 2024; date of current version 5 March 2024. This work was supported by the Wolfgang Gentner Programme of the German Federal Ministry of Education and Research under Grant 13E18CHA. *(Corresponding author: M. Janitschke.)*

M. Janitschke is with CERN, 1211 Geneva, Switzerland, and also with the University of Rostock, 18051 Rostock, Germany (e-mail: marvin.janitschke@cern.ch).

M. Bednarek, E. Ravaioli, A.P. Verweij, G. Willering, and M. Wozniak are with CERN, 1211 Geneva, Switzerland.

U. van Rienen is with the University of Rostock, 18051 Rostock, Germany.

Color versions of one or more figures in this article are available at https://doi.org/10.1109/TASC.2024.3366876.

Digital Object Identifier 10.1109/TASC.2024.3366876

TABLE I
MAIN CONDUCTOR PARAMETERS OF THE LHC MAIN DIPOLE [12], [13], [14], [15]

Parameter	Unit	Inner layer	Outer layer
Cable cross-section	mm^2	31.2	24.8
Number of strands	-	28	36
Copper/Nb-Ti	-	1.65	1.95
Strand diameter	mm	1.065	0.825
Strand twist pitch	mm	115	100
Filament twist pitch	mm	18	15
Filament diameter d_f	μm	7	6
RRR of copper matrix	-	190	

TABLE II
MAIN PARAMETER OF THE MAGNETS COMPONENTS [12], [13]

Component	Volume [m^3]	Material	Assumed ρ [Ωm]
Cold-bore	$3.4 \cdot 10^{-3}$	316 LN Steel	$720 \cdot 10^{-9}$
Copper wedges	$16.5 \cdot 10^{-3}$	OF copper C106	$0.54 \cdot 10^{-9}$
CPS	$3.7 \cdot 10^{-3}$	YUS 130S Steel	$400 \cdot 10^{-9}$

II. THE LHC MAIN DIPOLE

The LHC main superconducting dipole [12], [13], [14] is composed of two apertures connected in series, each with a differential inductance of L_{Ap}=49 mH at nominal conditions. The cross-section of one aperture is shown in Fig. 1. The magnet has a magnetic length of l_{mag}=14.3 m and generates a dipole field of B_{Nom}=8.0 T at nominal current I_{Nom}=11.85 kA and operating temperature T_{Nom}=1.9 K. The coils are wound using two different Nb-Ti Rutherford cables for the outer and inner layers, whose parameters are summarized in Table I.

Each coil block is separated from each other with metallic coil wedges (W). Moreover, the coils are covered for manufacturing reasons with 1 mm thick coil-protection sheets (CPS) before collaring. The coils are separated from the beam region by a 1.5 mm thick cold-bore (CB). Since these components are made of low-resistivity materials and are not laminated, considerable eddy currents are developed therein during a fast transient. Table II summarises their volumes, materials and assumed resistivities ρ [Ωm], and the components are highlighted in Fig. 1. Unlike magnets installed in the LHC machine, a beam-screen was not present during the measurements.

III. MODELLING APPROACH

A lumped-element network model has been developed, which aims to reproduce a superconducting magnet's electrical behavior. The model includes the magnet's inductances and stray capacitances as well as a coil resistance in case it is in the normal state. Each lossy, coupling effect is represented by a loop with an inductance L_{ec} [H] and resistance R_{ec} [Ω], coupled with a mutual inductance M_{ec} [H] to the magnets' inductance [16]. Moreover, all coupled inductors are also coupled with each other. As an example, a simplified electrical scheme of one dipole, showing the two apertures, each coupled to two coupling loops is shown in Fig. 2.

To derive the equivalent parameter of each coupling loop, the induced currents I_{ec} [A] and power loss P_{ec} [W] in the respective lossy volume, as well as the time constant τ_{ec} [s] of the loss

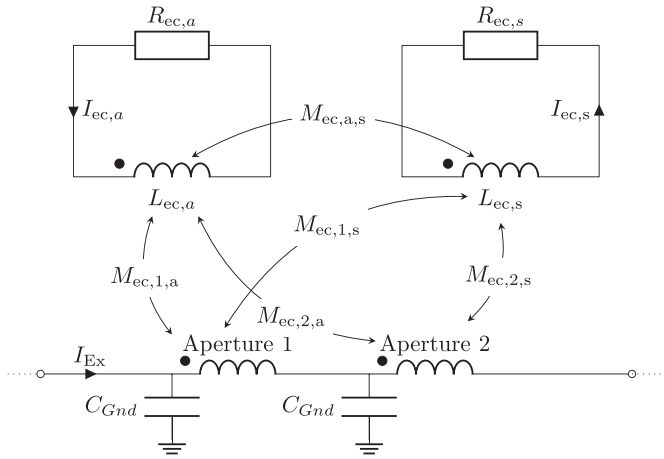

Fig. 2. Equivalent lumped-element network model, showing the modeling approach with two equivalent loops, coupled to the two magnet apertures.

TABLE III
TIME CONSTANTS OF THE CONSIDERED EFFECTS

	τ_{PC}	τ_{ISCL}	τ_{IFCL}	τ_W	τ_{CM}	τ_{CPS}	τ_{CB}
[ms]	-	110	37	4.5	0.35	0.093	0.03

mechanism, are needed. For a harmonic, sinusoidal excitation with the magnet current I_{Ex} [A], the equivalent parameters read:

$$R_{ec} = \frac{P_{ec}}{I_{ec}^2} \quad [\Omega] \tag{1}$$

$$L_{ec} = \tau_{ec} R_{ec} \quad [\text{H}] \tag{2}$$

$$M_{ec} = \frac{j\omega I_{ec} L_{ec} + R_{ec} I_{ec}}{j\omega I_{Ex}} \quad [\text{H}] \tag{3}$$

with j the imaginary unit and ω $\left[\frac{rad}{s}\right]$ the angular frequency. The time constants of each loop are summarized in Table III. The following paragraphs will describe the implementation of the main coupling effects.

A. Persistent Currents and Magnetization (PC)

Once the generated field penetrates into the superconducting filaments, instantaneous currents are induced in these, which oppose the penetration field and can persist until the superconductor transitions back into the normal conducting state [17], [18].

The effect on the magnet's differential inductance can be described in first approximation by the stored power in those currents [19], [20]:

$$P_{\text{Stored}} = \iiint_V H \frac{dB}{dt} dV \tag{4}$$

$$= \iiint_V \mu_0 \left(H \frac{dM}{dt} + H \frac{dH}{dt} \right) dV \tag{5}$$

where we used the relation $B = \mu_0(M + H)$ [T], with the vacuum permeability μ_0 $\left[\frac{\text{H}}{\text{m}}\right]$. Power loss due to magnetization heat for the small ΔB in the TFM is expected to be negligible.

The slope dM/dH, which is proportional to dI_{Ec}/dI_{Ex} [21], is approximately the same when the filaments are in virgin or magnetized state. Hence, the effect on the differential inductance is expected to be independent of the magnetization state. As these currents are instantaneous, it is also expected that the differential inductance of the magnet once transitioned into superconducting state, will reduce significantly [21], [22].

Due to the nature of this phenomenon, the equivalent resistance element is replaced by a current source. The equivalent inductance is derived by comparing the stored and lost power, and the equivalent network powers of the model [21].

B. Conductor Losses (CL)

The time-varying magnetic field generated by the sinusoidal excitation generates induced currents between the superconducting filaments. These currents are called inter-filament coupling currents and generate a field that opposes the applied field change. As these currents close through the conducting copper matrix of the strand, they generate a transitory loss (IFCL) [16], [23], [24], [25], [26]. Similarly, currents are also induced between the cable strands. These currents are called inter-strand coupling currents, closing through the strands' cross-contact resistances R_C [Ω] and hence causing losses (ISCL) [16], [23].

The superconducting filaments are usually enclosed in a copper sheath. The time-varying magnetic field applied to the strands also causes eddy currents to flow in this outer sheath of copper, generating additional losses (CML) [26].

In order to reduce model complexity, the derived parameters for all strands/turns are first binned based on the local magnetic field and then lumped together. The equivalent parameters for each bin are then the bin-averaged $\overline{R_{ec}}$ and $\overline{L_{ec}}$, with a mutual coupling of $M_{ec} = \sqrt{\sum_{n=1}^{n_t} M_{ec,n}^2}$ with $M_{ec,n}$ being all n_t mutual inductances in a bin, coupled to the inductance of the magnet's aperture. In this work, we used two bins per aperture, one for the outer and one for the inner layer.

Based on the calculated time constants of the three phenomena, IFCL and ISCL are expected to reduce the differential inductance in the lower frequency range, while the eddy currents in the outer copper sheath impact at higher frequencies, above 1 kHz.

C. Eddy Currents in the Magnets Metal Components (MC)

As the copper coil wedges, cold-bore, and the coil-protection sheets are made of conducting materials, the time-varying excitation field also induces eddy currents in these elements. The position and geometry of these components are complex, and there is no analytical derivation of induced current and loss. In order to include these effects, the respective components were modeled in a 2-dimensional FEM in COMSOL Multiphysics©. The time constants as well as frequency-dependent induced currents and losses were exported to calculate the equivalent frequency-dependent coupling parameters. The mutual coupling between the metal components is also simulated but assumed to be frequency-independent.

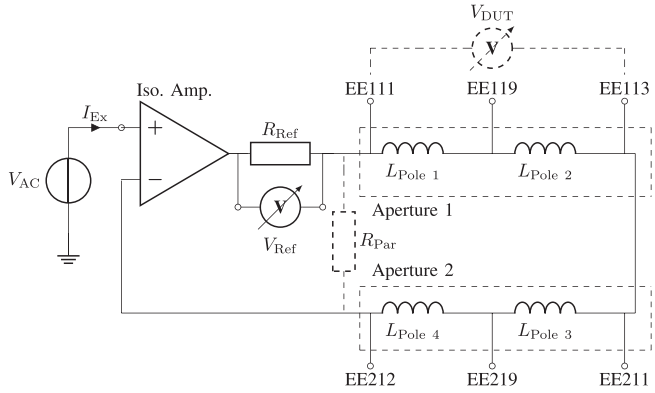

Fig. 3. Schematic showing the measurement set-up. The impedances are measured across various voltage taps (here shown for aperture 1).

Since the time constants of the eddy currents in these elements are smaller than a few ms, it is expected that they impact the magnet differential inductance for frequencies above 1 kHz.

IV. Measurement Set-Up

One spare main dipole was measured at the CERN magnet test facility. The measurements were performed with a gain/phase analyzer, which generates a sinusoidal excitation signal of amplitude $V_{\mathrm{AC}} = 10$ V with a maximum peak-to-peak current of $I_{\mathrm{Ex}} = 1$ A. This corresponds to a maximum field change in the centre of the aperture of about 0.7 mT. To reduce parasitic effects, the output signal of the generator is sent through an isolation amplifier, which isolates the measured signal from the ground and possible noise sources.

The schematic of the measurement set-up is shown in Fig. 3. The reference signal V_{Ref} [V] is measured across a reference resistor $R_{\mathrm{Ref}} = 25\ \Omega$. The desired signal V_{DUT} [V] is then measured between the respective voltage taps of interest. To reproduce the conditions in the LHC, all measurements were repeated with one resistor R_{Par}=100 Ω in parallel to both apertures [12]. The complex impedance was measured in the 1 Hz to 100 kHz frequency range with 20 points per decade. Using the complex-valued measurements, the impedance is calculated as $\mathbf{Z} = \frac{\mathbf{V}_{\mathrm{DUT}}}{\mathbf{V}_{\mathrm{Ref}}} \cdot R_{\mathrm{Ref}}$ [Ω].

In order to measure the effect of different magnetization states of the superconducting filaments, the impedance was also measured just after cool-down ("virgin" magnet) and after one magnetic cycle to nominal current and back. This cycle ensured that nearly all filaments were completely saturated, as the field was well above the penetration field of the dipole strands $B_{\mathrm{p}} = \frac{\mu_0 J_C(T,B) d_f}{\pi}$ [T], with $J_c\left[\frac{\mathrm{A}}{\mathrm{m}^2}\right]$ the critical current density of the filament [23]. The measurements were also done continuously during the natural warm-up.

V. Model Validation

The measurements were used to validate the proposed features of the model in the frequency range below 5 kHz, which is most relevant for accelerator magnets, operating in the range of a few mHz. The measured impedance magnitude over this frequency

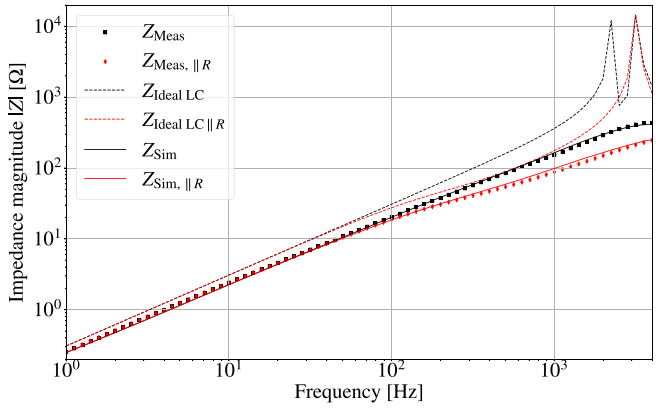

Fig. 4. Measured impedance magnitude of the LHC main dipole versus the simulation of the equivalent network model, with and without R_{Par}.

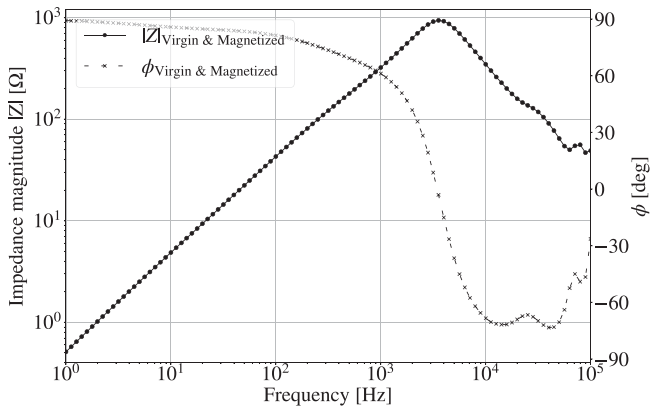

Fig. 5. Measured modulus and phase of the complex impedance of the LHC main dipole in virgin and fully magnetized state, which fully overlap.

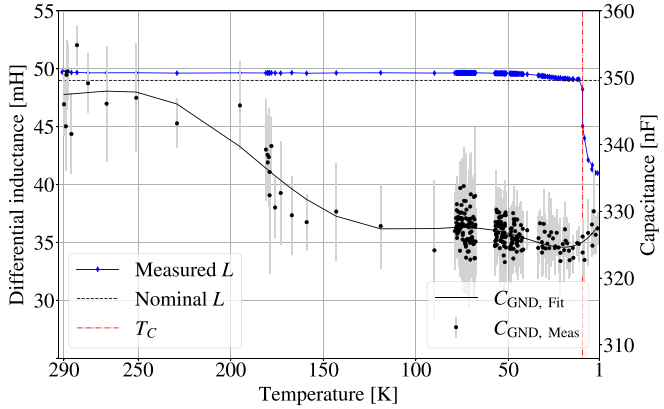

Fig. 6. Measured inductance of the two apertures and cubic spline-fitted capacitance from different voltage taps to ground.

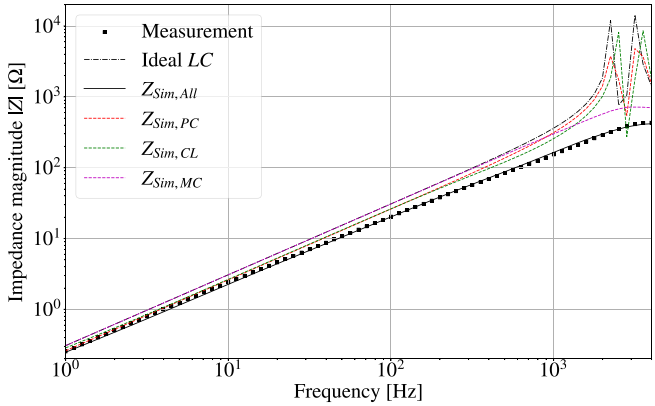

Fig. 7. Measured complex impedance of the LHC main dipole versus the simulated impedance of the equivalent network model.

range compared to the simulated one is shown in Fig. 4. In order to reflect the real conditions in the LHC, simulations and measurements with R_{Par} are also shown. The agreement between simulation and measurement is good throughout the entire frequency range, with an average error below 3.5%. The average error with respect to a simulation not including non-linear effects would range above 50%.

The measured transfer functions for the case of a virgin and fully magnetized magnet are shown in Fig. 5. As expected by the model, both measurements are identical at all measured frequencies, with an error within the error range of the measurement set-up. The TFM also validates the persistent current and magnetization model feature over temperature. The measured inductance and capacitance, calculated from the low- and high-frequency reactances, respectively, are shown in Fig. 6. Due to thermal contractions and permittivity changes, the capacitance and inductance drop from about 350 nF to 330 nF and from about 50 mH to the nominal 49 mH, respectively. One can observe the sudden drop of inductance, due to superconducting effects in the filaments, once the magnet coil transitions into the superconducting state.

Finally, Fig. 7 shows the contributions of the effects to the final simulation results. The persistent currents reduce the differential inductance of the magnet at low frequencies and explain the measured, reduced inductance with an error of less than 1%. The conductor losses impact the impedance of the magnet only at slightly higher frequencies, in the range of a few Hz up to about 1 kHz. This can be observed by the simulated impedance kink in these frequencies, including the conductor loss contribution. The conductor losses and the filament currents provide a very good agreement between measurement and simulation at frequencies up to about 1 kHz. However, the impedance above 1 kHz is strongly influenced by the eddy currents in the magnet's metal components due to their smaller time constants.

VI. Conclusion and Outlook

A physics-driven lumped-element electrical model, which includes multiple non-linear, interdependent coupling effects in a superconducting magnet, was described. A transfer function measurement campaign on a spare LHC main dipole at the CERN magnet test facility was described and provided data to validate the model in the frequency domain. It is shown that the proposed model is capable of accurately reproducing the LHC main dipole transfer function in a frequency range up to 5 kHz. Moreover, the model accurately captures the effects due to instantaneous superconducting filament magnetization states, which were observed in the temperature-dependent measurements. The validated model can be used to investigate further behaviour of the dipole, for example, to simulate different

electrical non-conformities and to evaluate their impact on the magnet performance.

ACKNOWLEDGMENT

The authors would like to thank the CERN SM18 team for their help in the measurements, in particular, R. Bouvier and G. Ninet.

REFERENCES

[1] H. Ehmler et al., "Comparative analysis of impulse and impedance tests to detect short circuits within the W7-X magnets," *IEEE Trans. Appl. Supercond.*, vol. 16, no. 2, pp. 767–770, Jun. 2006.

[2] K. Rieße, T. Rummel, G. Ehrke, and M. Koppen, "Design, tests, and repair procedures for the electrical insulation of the superconducting W7-X magnets," *IEEE Trans. Appl. Supercond.*, vol. 20, no. 3, pp. 447–450, Jun. 2010.

[3] H. Ehmler, I. R. Dixon, T. A. Painter, and J. A. Powell, "Electrical AC tests on CICC coil for series-connected hybrid magnet," *IEEE Trans. Appl. Supercond.*, vol. 22, no. 3, Jun. 2012, Art. no. 9002204.

[4] A. Foussat, L. Grand-Clement, D. Smekens, F. O. Pincot, L. Bortot, and F. Savary, "Frequency-domain diagnosis methods for quality assessment of Nb3Sn coil insulation systems and impedance measurement," *IEEE Trans. Appl. Supercond.*, vol. 28, no. 3, Apr. 2018, Art. no. 4003505.

[5] R. E. Shafer, "Eddy currents, dispersion relations, and transient effects in superconducting magnets," FERMILAB, Batavia, IL, USA, Tech. Rep. FERMILAB-TM-991, Sep. 1980. [Online]. Available: http://cds.cern.ch/record/192894

[6] K. M. Smedley and R. E. Shafer, "Experimental determination of electrical characteristics and circuit models of superconducting dipole magnets," *IEEE Trans. Magn.*, vol. 30, no. 5, pp. 2708–2712, Sep. 1994.

[7] K. Dahlerup-Petersen and F. Schmidt, "Impedance measurements and modeling of the ten metre prototype LHC dipole magnet," CERN, Geneva, Switzerland, Tech. Rep. LHC-Project-Note-11, Oct. 1995. [Online]. Available: https://cds.cern.ch/record/692033

[8] F. Bourgeois and K. Dahlerup-Petersen, "Methods and results of modeling and transmission-line calculations of the superconducting dipole chains of CERN's LHC collider," CERN, Geneva, Switzerland, Tech. Rep. LHC-Project-Report-497; CERN-LHC-Project-Report-497, Aug. 2001. [Online]. Available: https://cds.cern.ch/record/592974

[9] M. Martino, "Low-frequency analytical model of superconducting magnet impedance," *Modelling Simul. Eng.*, vol. 2022, Nov. 2022, doi: 10.1155/2022/2105847.

[10] A. F. Wolstrup, E. Ravaioli, T. G. Zsurzsan, and Z. Zhang, "Automatic frequency-domain modelling of superconducting magnets and its usability to model general inductors," in *Proc. IEEE 12th Energy Convers. Congr. Expo. Asia*, 2021, pp. 1312–1318.

[11] E. Ravaioli, K. Dahlerup-Petersen, F. Formenti, J. Steckert, H. Thiesen, and A. Verweij, "Modeling of the voltage waves in the LHC main dipole circuits," *IEEE Trans. Appl. Supercond.*, vol. 22, no. 3, Jun. 2012, Art. no. 9002704.

[12] O. Brüning et al., "LHC design report," CERN, Geneva, Switzerland, Tech. Rep. CERN-2004-003-V-1, 2004. [Online]. Available: https://cds.cern.ch/record/782076

[13] L. Rossi, "The LHC main dipoles and quadrupoles toward series production," *IEEE Trans. Appl. Supercond.*, vol. 13, no. 2, pp. 1221–1228, Jun. 2003.

[14] E. Ravaioli et al., "First implementation of the CLIQ quench protection system on a 14-m-long full-scale LHC dipole magnet," *IEEE Trans. Appl. Supercond.*, vol. 26, no. 4, Jun. 2016, Art. no. 4000505.

[15] Z. Charifoulline, "Residual resistivity ratio (RRR) measurements of LHC superconducting NbTi cable strands," *IEEE Trans. Appl. Supercond.*, vol. 16, no. 2, pp. 1188–1191, Jun. 2006.

[16] E. Ravaioli, B. Auchmann, M. Maciejewski, H. ten Kate, and A. P. Verweij, "Lumped-element dynamic electro-thermal model of a superconducting magnet," *Cryogenics*, vol. 80, pp. 346–356, 2016. [Online]. Available: http://www.sciencedirect.com/science/article/pii/S0011227516300832

[17] C. P. Bean, "Magnetization of hard superconductors," *Phys. Rev. Lett.*, vol. 8, pp. 250–253, Mar. 1962. [Online]. Available: https://link.aps.org/doi/10.1103/PhysRevLett.8.250

[18] Y. B. Kim, C. F. Hempstead, and A. R. Strnad, "Magnetization and critical supercurrents," *Phys. Rev.*, vol. 129, pp. 528–535, Jan. 1963. [Online]. Available: https://link.aps.org/doi/10.1103/PhysRev.129.528

[19] M. Sorbi and V. Marinozzi, "Magnetization heat in superconductors and in eddy current problems: A classical thermodynamic approach," *IEEE Trans. Appl. Supercond.*, vol. 26, no. 6, Sep. 2016, Art. no. 4901509.

[20] E. Ravaioli, B. Auchmann, and A. P. Verweij, "Fast method to quantify the collective magnetization in superconducting magnets," *IEEE Trans. Appl. Supercond.*, vol. 23, no. 3, Jun. 2013, Art. no. 4700204.

[21] E. Ravaioli, "Persistent-currents magnetization in STEAM-LEDET," CERN, Geneva, Switzerland, Tech. Rep. EDMS 2418186, 2020.

[22] E. Ravaioli, A. P. Verweij, and H. H. J. ten Kate, "Unbalanced impedance of the aperture coils of some LHC main dipole magnets," *IEEE Trans. Appl. Supercond.*, vol. 23, no. 3, Jun. 2013, Art. no. 400010.

[23] A. P. Verweij, "Electrodynamics of superconducting cables in accelerator magnets," Ph.D. dissertation, Univ. Twente, Twente, The Netherlands, 1995. [Online]. Available: https://cds.cern.ch/record/292595

[24] M. Wilson, *Superconducting Magnets* (Series Monographs on Cryogenics). Oxford, U.K.: Clarendon Press, 1983.

[25] W. J. Carr, "AC loss in a twisted filamentary superconducting wire," *J. Appl. Phys.*, vol. 45, no. 2, pp. 929–938, 1974. [Online]. Available: http://scitation.aip.org/content/aip/journal/jap/45/2/10.1063/1.1663341

[26] B. Turck, "Losses in superconducting multifilament composites under alternating changing fields," Los Alamos Nat. Lab., Los Alamos, NM, USA, Tech. Rep. LA-7639-MS, 1979. [Online]. Available: https://www.osti.gov/biblio/6165478